Graphene, graphene oxide and reduced graphene oxide as pH sensitive sensor materials

P. Salvo[1,2]*, B. Melai[2], N. Calisi[2], C. Paoletti[2], F. Bellagambi[2], A. Kirchhain[2], M. G. Trivella[1], R. Fuoco[2], F. Di Francesco[2]

[1]Institute of Clinical Physiology, National Research Council, Via Moruzzi 1, 56124, Pisa, Italy.

[2]Department of Chemistry and Industrial Chemistry, University of Pisa, Via Moruzzi 13, 56124, Pisa, Italy.

*pietro.salvo@gmail.com; Tel.: +39 0503152703.

Abstract

pH measuring and monitoring is fundamental to understand or control many chemical processes in biological, industrial or environmental fields. The state-of-the-art pH sensor is the glass electrode, but single-use paper strips are also widely used and there are also a few ion-selective field effect transistors (ISFETs). Due to the excellent properties of graphenic materials, new pH sensors can be fabricated that fulfil the increasing request for lightweight, miniaturized and cost-effective products. This review describes how graphene, graphene oxide and reduced graphene oxide can be used as sensitive materials for pH sensors. The various configurations are reported along with the advantages and current limitations.

Introduction

pH governs many chemical reactions in nature. Biology, environmental protection, food quality control, medicine and industry are just a few fields where pH sensors have been extensively used to understand the nature of chemical processes, as well as how to monitor the quality and control the safety [1-6]. Although paper test strips and glass electrodes remain the most widespread pH sensors, many studies have focused on developing less fragile, miniaturized, and biocompatible sensors, with a better signal-to-noise ratio (SNR). The pH signal can be transduced through various techniques and technologies, e.g. potentiometry, optics, and ion-selective field effect transistors (ISFETs).

Illustrative pH-sensitive materials reported in the literature include polyaniline (PANI), polypyrrole (PPy), polyparaphenylenediamine, poly(vinyl pyridine), poly(methacrylic acid) (PMAA), poly(acrylic acid) (PAA), palladium oxide, aluminium oxide, riboflavin, anthraquinonesulfonate, fluorescent dyes such as rhodamine, silicates and silanes, 6-carboxyfluorescein, as well as seminaphthorhodafluor (SNARF)/seminaphthofluorescein (SNAFL), hydrogels such as hydroxyethyl methacrylate/dimethylaminoethyl methacrylate (HEMA-DMAEMA) and poly(vinyl alcohol)/poly(acrylic acid) (PVA-PAA) [7-27].

Despite the high number of materials and devices reported in the literature, only a few have been marketed. The most challenging hurdles are the degradation of materials, low sensitivity, drift and difficulties in mass production. ISFETs are currently the most effective alternative to glass electrodes. Stable and low drift pH-ISFETs suitable for long use are on the market, such as the DuraFET® sensor by Honeywell. However, although the DuraFET®'s sensing element is only a few millimetres wide, the probe is longer than 15 cm and impractical, for example, for *in vivo* biosensing[28]. A multi-purpose and high performance micro/nano sensor is the holy grail for pH measurement.

After the isolation of graphene from highly oriented pyrolytic graphite in 2004 at the University of Manchester[29], many researchers started to investigate how to exploit the extraordinary electrical, chemical, mechanical and optical properties of this material for

sensing and biosensing[30-33]. The first section of this review focuses on the chemico-physical properties and mechanisms that underlie graphene's sensitivity to pH as well as pH sensors exploiting such properties.

Graphene oxide (GO) resulting from the oxidation of graphite is the precursor of reduced graphene oxide (rGO), i.e. graphene obtained by the exfoliation and reduction of GO[34]. GO sensitivity to pH depends on the surface hydroxyl (OH), carboxyl (COOH) and epoxy groups (COC) that protonate/de-protonate when pH changes: GO and its applications for pH sensing are discussed in the second section of this review. Although reduced graphene oxide shares many of graphene's physical and chemical properties, there are differences such as the presence of defects and residual oxygen atoms not removed by reduction[35] that justify discussion in a separate section. In the literature, graphene, GO and rGO are often mixed with other compounds to obtain pH sensitive materials, mainly to improve the mechanical structure or the electrical conductivity of the resulting composite.

This review only reports devices where graphene, GO or rGO are used as the main pH sensitive element. We provide an overview of research efforts in the last decade and trends for the development and enhancement of graphene-based pH sensors.

Graphene

Solution-gated ISFETs

A typical configuration of a graphene-based ISFET is the solution-gated FET (SGFET), where the graphene is used as the conduction channel. The SGFET resembles a three-electrode electrochemical cell, where the electrolyte solution is in direct contact with

graphene (working electrode), the gate voltage (V_G) is applied through a reference electrode (Ag/AgCl, calomel or Pt), and a Pt counter electrode completes the device. Although the counter electrode is often absent, this top-gated FET with Ti/Au or Cr/Au contacts for source and drain is a common configuration for pH measurement (Fig. 1a). The most common methods for fabricating the graphene channel are the exfoliation of graphite and the epitaxial growth, typically by chemical vapour deposition (CVD). After the CVD of carbon atoms on a substrate such as copper, the graphene film is coated with a protective material, e.g. poly(methyl methacrylate) (PMMA) or poly(dimethylsiloxane) (PDMS), then the substrate is etched and the film is transferred onto the ISFET substrate, e.g. SiO_2/Si or 6H-SiC.

In 2008, Ang *et al.* proposed an SGFET to measure pH including an epitaxial graphene layer grown on 6H-SiC[36]. Ang *et al.* hypothesized conductivity (σ) of the graphene channel to be modulated by the adsorption of hydroxyl (OH^-) and hydroxonium (H_3O^+) ions onto the surface. They used a $V_G \in [-1, 1]$ V and a constant drain–source voltage (V_{DS}) of -1 V, and observed that OH^- bound at the inner Helmholtz plane of the graphene/solution interface attracted their counterions in graphene in the case negative V_G, thus inducing a p-type doping. On the other hand, n-type doping was induced by the H_3O^+ adsorption in the case of positive V_G or acid pH. As pH increased from 2 to 12, the Dirac voltage (V_{Dirac}, i.e. the voltage at which the number of holes and electrons is balanced and the channel conductance is minimum) showed a positive shift (Figs. 1b, 1c), thus allowing the pH to be measured. Surprisingly, for negative V_G and 3-4 graphene layers, a sensitivity of about 99 mV/pH was found, which is greater than the Nernst limit of 59.16 mV/pH.

Lei *et al.* fabricated a chemiresistor, i.e. a gate-free FET, with a graphene sheet exfoliated from graphite and deposited onto a SiO_2/Si substrate[37]. For a constant current of 10 μA and an initial resistance of 86 KΩ, the sensitivity of the device from pH 4 to 10 was approximately 2.13 KΩ/pH. The resolution was calculated as the ratio between the maximum standard

deviation of resistance for multiple measurements and the sensitivity of the device. The resolution at basic pH and acid pH were 0.33 and 0.97, respectively. This behaviour may be explained assuming that the OH^- are more ordered on the inner Helmholtz plane than the H_3O^+. This sensor was reusable despite a hysteresis of about 2 KΩ. The authors suggested that reusability was probably related to the easy removal of electrolytes from graphene due to its extremely low thickness, although the paper did not report any precise value or further explanation. Lee *et al.* proposed another example of a gate-free FET, this time on a paper substrate[38]. Graphene was dispersed in sodium dodecyl sulfate (SDS) and, after sonication, the dispersion was poured onto a paper substrate through a metal mask under vacuum. After rinsing with deionized water and drying at 80 °C for 20 min, six U-shaped graphene sensors were fabricated. A paraffin pen was used to define a closed measurement area around each sensor. The highest fabrication repeatability and electrical stability were obtained by depositing 0.5 mg of graphene dispersion through vacuum filtration, which resulted in a sensing layer thickness of about 100 µm. The response was measured from pH 1 to about 10.5 by dispensing 10 µL drops of different buffer solutions in each of the six measurement areas. At $V_{DS} \in [-1, 1]$ V, the sensitivity was about 30.8 Ω/pH and the correlation between resistance and pH resulted in a regression line with a coefficient of determination $R^2 \cong 0.93$.

Following the same structure as Fig. 1a, Ohno *et al.* described a FET with a single layer of graphene and a leakage current lower than 10 nA[39]. The conductance was measured for two FET configurations: top-gate and back-gate, where the back-gate is an n-doped Si substrate. The top-gate capacitance was three times greater than in the back-gate configuration, therefore confirming the top-gate as the preferred option for sensing. The V_{Dirac} positively and linearly shifted at increasing pH from 4 to 8.2. For $V_G \in [-50, 50]$ mV, the sensitivity was about 30 mV/pH. The authors pointed out that the V_{Dirac} may shift at different

pH values because of charged impurities scattering, which can be caused, for example, by the residual resist used in the photolithographic fabrication process, or graphene defects.

Ristein *et al.* used a monolayer of graphene on a 6H–SiC single crystal[40]. The solution-gated FET (SGFET) had a leakage current lower than 1 nA and linear I–V characteristics up to $|V_{DS}| = 0.1$ V. The drain-source current (I_{DS}) versus V_G was measured at $V_{DS} = -50$ mV from pH 3 to 12. The V_{Dirac} shift per unit pH, i.e. the sensitivity, was 19 ± 1 mV/pH. The authors compared the conductivity of the graphene channel (3.5×10^{-5} S) with the value reported by Ang *et al.* (3.5×10^{-4} S) since their transistors were similar. The difference of one order of magnitude in conductivity was probably because Ang *et al.* tested their SGFET at $V_G > 0.3$ V, which Ristein *et al.* found to be the maximum voltage that would prevent defects in the graphene layer. These defects probably caused the formation of holes, which then led to a super-Nernstian sensitivity.

Cheng *et al.* etched an SiO_2 substrate to suspend a graphene layer shorter than 1 µm between the Cr/Au contacts of drain and the source[41]. The resulting FET led to a V_{Dirac} of 0.1 ± 0.2 V and to a larger conductivity at negative V_G (majority of holes) compared to positive V_G (majority of electrons). Compared with a standard configuration, there was a net improvement in the FET characteristics with the suspended graphene: the SNR increased by 14 dB at frequencies below 1 KHz, and the sensitivity increased 1.5 and 2 times for holes and electrons, respectively, leading to a symmetric σ-V_G curve. These improvements were ascribed to a reduced scattering, but a full explanation was not supplied. This FET had a sensitivity of about 17 mV/pH when tested with buffer solutions from pH 6 to 9 and $V_G \in [-50, 50]$ mV.

Studies on the effects of different electrolyte solutions have further contributed to the comprehension of the mechanisms regulating the graphene response to pH. Lee *et al.* investigated the V_{Dirac} shift when an SGFET was exposed to sodium hydroxide (NaOH), hydrochloric acid (HCl) and potassium hydroxide (KOH)[42]. A graphene film was grown onto

158 a copper film in a furnace at 1000 °C in presence of a mixture of CH_4 and H_2. PMMA
159 dispersed in chlorobenzene was used to coat and transfer the graphene layer onto a Si/SiO_2
160 wafer after copper etching. The wafer had pre-patterned source, drain and Cr/AU electrodes.
161 PMMA was removed by rinsing the device with a solution of acetone and deionized water,
162 whereas graphene was patterned with standard photolithographic techniques. Solutions at
163 different pH values in the range [6, 8] were obtained with different concentrations of Na^+, Cl^-
164 and K^+ in 0.05 M phosphate solutions (Table 1).
165
166 While the SGETs reported in other works had positive V_{Dirac} shifts at increasing pH, Lee *et*
167 *al.*'s transistor showed a negative V_{Dirac} shift which depended on the ionic composition and
168 strength of the buffer solutions. At V_{DS} = 50 mV, $V_G \in [0, 1]$ and for pH 6, 7 and 8, the pH
169 sensitivities were -78, -38 and -7 mV/pH in buffer solutions containing different
170 concentrations of Na^+, Cl^- and K^+ respectively, whereas the sensitivity was +69 mV/pH in
171 reference buffers (0.05 M). Therefore, a negative shift for increasing pH was observed in the
172 lab-made buffers containing the electrolytes and a positive shift in commercial reference
173 buffers. This result could not be explained in terms of ionic strength as the response for
174 sodium and potassium buffers were very different, although the ionic strengths were
175 identical. The type of ion played an important role, as the V_{Dirac} shift was more sensitive to
176 the concentration of Na^+ than to the concentrations of Cl^- or K^+. Lee *et al.* hypothesized that
177 the shift in V_{Dirac} was a consequence of the ionic charge screening, which depends on ion
178 size, degree of hydration, and affinity towards the graphene surface. They suggested pH
179 measurements should only be performed in diluted solutions, as ionic charge screening is
180 more significant at high concentrations. In fact, their tests with five and ten times diluted
181 sodium solutions yielded the typical positive V_{Dirac} shift for increasing pH, whereas the sensor
182 increased its sensitivity from -7 to -27 mV/pH in a 0.1 M potassium solution.

Heller *et al.* expanded this research by using different KCl concentrations buffered at pH 7 and demonstrating a linear dependence between the V_{Dirac} shift and the log(KCl) concentration with respect to the V_{Dirac} normalized to its value at 1 M KCl in the range [1 mM, 1 M][43]. Similar results were obtained with LiCl at pH 3. At high ionic strength, the double layer capacitance at the interface graphene-buffer increases and the surface potential decreases. At pH 7, the V_{Dirac} shift changed by -42.7 mV/decade with the buffer concentration. At pH 3, there was a sign inversion (+18.9 mV/decade), probably because of the supporting SiO_2 layer. In fact, SiO_2 has ionized silanol and silylamine groups, such as SiO^-, $SiOH_2^+$ and $SiNH_3^+$, which can negatively or positively charge the surface. The effect of different ions on the measurement of pH was confirmed by testing Li^+, K^+ and tetraethylammonium (TEA^+), but an explanation of this effect has still to be found. However, Heller *et al.* hypothesized that the ionic radius or a specific adsorption onto graphene could play a major role.

Fu *et al.* (ref. 44) pointed out that the range of graphene sensitivities to pH reported in the literature was very large (12–99 mV/pH). They thus set up an experiment with the three-electrode configuration shown in Fig. 1a. Graphene was exfoliated or grown on copper by chemical vapour deposition and then transferred to the SiO_2/Si substrate. For $V_{DS} \in [10, 50]$ mV and $V_G \in [0.1, 0.8]$ V, the leakage current (1 nA) was negligible compared with the measured I_{DS}. Although the V_{Dirac} shifted positively at increasing pH (as in previous works), the sensitivity was only 6 ± 1 mV/pH from pH 5 to 10. The hydrophobicity of the graphene surface was then increased by adding fluorobenzene for 30 s and drying the FET. In this case, the sensitivity was almost zero from pH 4 to 10. On the other hand, when an Al_2O_3 layer thinner than 2 nm was deposited (atomic layer deposition, 100 °C) on graphene, the sensitivity increased to 17 mV/pH from pH 3 to 8. According to Fu *et al.*, OH functional groups from Al_2O_3 turned graphene partially hydrophilic. Their conclusion was that a defect-free graphene is not able to sense pH, and that graphene response to pH depends on the

presence of imperfections, such as the hydroxyl and carbonyl groups. The sensitivities of 99 and 20 mV/pH reported in (ref. 36) and (ref. 41), respectively, probably depended on a high leakage gate current.

Kwon *et al.* investigated the role of defects in graphene mesh FETs (GM-FETs)[45]. The mesh structure was synthesized using silica spheres as a growth mask to avoid photolithographic patterning, thereby reducing the disorder and contamination of carbon atoms. A hexagonal close-packed monolayer of silica spheres covered a copper foil as well as the graphene mesh aroused from the dissociation of carbon atoms at the copper−silica interface. The resulting mesh was a hexagonal array of circular holes with an average diameter and interspacing of 300 and 600 nm, respectively. At different pH values from 6.55 to 8.25 and with V_{DS} = 50 mV, the GM-FETs had a sensitivity of about 90 mV/pH. The authors suggested that this super-Nernstian sensitivity could depend on a high number of unsaturated carbon atoms at edge defects, which could adsorb or probably bind the H^+ ions. Although the formation of covalent bonds improved sensitivity, the irreversibility of this reaction could limit the use of GM-FETs. In fact, sensitivity decreased to about 7 mV/pH after five cycles of 3 min tests of the GM-FETs in solutions at pH 8.25, 7.85, 7.40, 6.95, and 6.55. Therefore, it is essential to control graphene defects in order to obtain reproducible and reliable results.

As the edges of graphene are chemically reactive, Tan *et al.* patterned the graphene layer by electron-beam lithography (EBL) and oxygen plasma into four columns of 99.1 ± 1.5 nm wide and 5.5 μm long nanoribbons (GNRs) to improve the number of hydroxyl groups[46]. With a constant V_{DS} = 10 mV, sensitivity improved after patterning from about 6.5 to 23.6 mV/pH in the pH range [6, 8]. One advantage of the edges defects is that unlike defects in the basal plane they do not affect the current flow in the graphene channel. Tan *et al.* also found that the improvement did not depend on impurities such as residual PMMA used in the photolithographic process, since similar results were obtained when hydrogen silsesquioxane (HSQ) was used as the photoresist.

Zhang *et al.* combined the ideas exposed in (refs 41, 46) in order to improve the graphene sensitivity to pH and fabricate a suspended GNR ISFET for measuring pH and cancer markers in solution[47]. In this study, the width of GNRs was 50 nm and the GNR ISFET was powered with V_{DS} = 1 V, whereas $V_G \in$ [-1,8, 1.8] V. The I_{DS} was normalized with respect to the current I_0 at pH 9 and presented as the ratio $(I_{DS}- I_0)/I_0$. From pH 5 up to 9, the suspended GNR FET was 1.5 times more sensitive (about 25 mV/pH) than an unsuspended GNR FET and a normal SGFET. However, as reported in (ref. 40), those voltages could lead to the formation of defects capable of altering the measurement.

The electrochemical characteristics of crystalline epitaxial graphene grown on SiC were studied in (ref. 48) using a three-electrode electrochemical cell consisting of a graphene coated working electrode, an Ag/AgCl reference electrode with saturated KCl and a Pt wire as counter electrode. Graphene was anodized at 2 V in a pH 7 phosphate buffer solution to introduce oxygenated surface groups such as C=O and C–O–H. X-ray photoelectron spectroscopy (XPS) established that long anodization times (e.g. 500 s) led to the functionalization of the edges with hydroxyl and carboxylic groups. The hydroxyl and carboxylic groups increased the capacitive charging current, thus fastening the electron transfer kinetics. The sensitivity to pH was determined with the Mott-Schottky equation, which is commonly used to study the electrochemical interface between a semiconductor and an electrolyte solution[49]. The total capacitance at the interface between graphene and an electrolyte solution is given by the sum of the reciprocals of the Helmholtz layer capacitance (C_H) and the space-charge capacitance of graphene (C_G). The typical assumption is that $C_H >> C_G$ so that the Mott-Schottky equation becomes:

$$\frac{1}{C_G^2} = \frac{2}{\varepsilon\varepsilon_0 eN}\left(V - V_{FB} - \frac{kT}{e}\right) \qquad (1)$$

where ε is the dielectric constant of graphene, ε_0 is the vacuum permittivity, e is the electron charge, N is the donor density (holes or electrons), V is the applied potential, V_{FB} is the flat-band potential (i.e. the potential at which the conduction and the valence bands of graphene are flat), k is the Boltzmann constant, and T the temperature. When pH changed from 2 to 10, $\Delta V_{FB} = V_{FB}(pH = 10) - V_{FB}(pH = 2)$ for pristine graphene was much lower (0.1 V) than for the anodized graphene (0.41 V). This result was reflected in a pH sensitivity of 12.5 mV/pH for pristine graphene and 51.3 mV/pH for anodized graphene. The better performance of anodized graphene thus depended on the presence of the hydroxyl and carboxylic groups.

The works described so far highlight that graphene-based FETs have ambipolar characteristics, i.e. the charge carriers in the graphene channel were holes or electrons depending on whether the V_G was smaller or greater than the V_{Dirac}. Nevertheless, Zuefuddin *et al.* presented in 2013 an FET that was p-doped in the range $V_G \in$ [-30, 30] V[50]. However, this voltage range seems too wide and probably caused some defects in graphene. A monolayer graphene was obtained by the decomposition of CH_4 in a CVD reactor onto a $Cu/SiO_2/Si$ substrate. After etching the copper with $FeCl_3$, graphene was transferred onto SiO_2/Si and an array of FETs were fabricated using standard microlithography. The authors suggested that the absence of a V_{Dirac} could depend on the p-doping from residuals left during the transfer process, but the type of resist was not reported. The sensitivity to pH was tested with different buffer solutions and there was an I_{DS} shift of 5% and 10% at pH 5.1 and 8.2, respectively. The repeatability and hysteresis were not reported.

Lin *et al.* used CVD on copper and nickel foils to grow graphene, which was then suspended on an array of Cr/Pb sources and drains onto a SiO_2/Si substrate[51]. The channel width was 20 µm. The graphene grown onto nickel (Gr_{Ni}) was a continuous film with a low number of defects and consisted of less than 10 layers, whereas the graphene grown on copper (Gr_{Cu}) was a quasi-continuous film consisting of a single-crystal monolayer. Since I_{DS} had an

285 exponential decay over time, the response was measured as (I_{DS}- I_{DSin})/ I_{DSin}, where I_{DSin}
286 was the initial value. The Gr_{Ni} was tested at pH 7, 10, 11 and 13 and showed a linearly
287 increasing response for increasing pH (4.75% at pH 7, 45.1% at pH 13, and 0.1 pH
288 resolution). At V_G = 0 V and V_{DS} = 0.1 V, the I_{DSin} was not constant at different pH values
289 (e.g. about 250 µA at pH 7 and 1.5 mA at pH 13), thus indicating an irreversible adsorption
290 of ions on graphene. The Gr_{Cu} was used at pH 7.35, 7.59 and 7.86 with sensitivities of
291 34.5%, 47.6%, and 57.4%, respectively. The resolution was 0.01 pH. However, their paper
292 does not report the number of measurements nor the error bars on plots.
293 The adsorption of ions onto a graphene surface and desorption have been studied via the
294 effect on graphene conductivity. Kiani *et al.* proposed an analytical model to explain and
295 predict the effect of electron exchange for a monolayer GNR[52]. The model used a typical
296 ISFET configuration with gold contacts, SiO_2/Si substrate and an Ag/AgCl reference
297 electrode. The conductance (G) of a GNR can be written as:
298

$$G = \frac{3q^2\sqrt{3\pi a^3 t^3 k_B T}}{hl}\left[F_{-1/2}(\eta) + F_{-1/2}(-\eta)\right] \qquad (2)$$

299
300 where q is the electron charge, a is the graphene lattice constant (0.246 nm), t = 2.7 eV is
301 the tight-binding energy for the nearest neighbour C-C atoms, k_B is the Boltzmann constant,
302 T is the temperature, h is the Planck constant, l is the graphene channel length, η =
303 $(E_F - E_g/k_B T)$ is the normalized Fermi energy (E_F is the Fermi level and E_g is the band gap
304 energy), and $F_{-1/2}$ is Fermi-Dirac integral of order $-1/2$. The conductance at different pH
305 (G_{pH}) was modelled as $G_{pH} = \frac{P}{pH}G$.
306 The parameter P is the pH sensing factor and, at T = 25°C, can be calculated as $P =$
307 $\alpha \ln(pH) + \beta$, where α and β are 2.7318 and 4.5044, respectively. This model showed a
308 good agreement with experimental data from the authors (i.e. Kiani *et al.*) and (ref. 44).

Although the model was not sufficiently precise to fit the V_{Dirac}, the pH sensing factor can be used to predict the conductance of the graphene channel when exposed to an electrolyte solution.

Solution-gated ISFETs on a flexible substrate

The SiO_2/Si is widely used as substrate for the fabrication of graphene-based ISFETs. However, an attempt has been made to produce these ISFETs on flexible substrates to develop a technology capable of providing lightweight, bendable and/or stretchable, potentially environment-friendly and cost effective devices. Mailly-Giacchetti *et al.* compared the performances of an SGFET fabricated on SiO_2/Si with a similar device on a 125 µm thick poly(ethylene 2,6-naphthalenedicarboxylate) (PEN) substrate[53]. Monolayer graphene films were grown on copper foils by CVD and then transferred onto SiO_2/Si and PEN. Two SiO_2/Si SGFETs were fabricated with and without moderate PMMA leftover in order to study the effects of residues due to the microlithographic process. The leakage current for both SiO_2/Si and PEN SGFETs was about 1 nA. The tests on pH in the range [4, 8] were performed at V_{DS} = 50 mV and $V_G \in$ [-0.1, 0.5] V. The SiO_2/Si SGFETs with (SGFET-SiO_2-PMMA) and without (SGFET-SiO_2) residues showed a positive V_{Dirac} shift at increasing pH with similar sensitivities, i.e. 21 and 22 mV/pH respectively. The SGFET-SiO_2 was more p-doped than the SGFET-SiO_2-PMMA, probably because of the annealing step at 500 °C in H_2/Ar to remove PMMA. The PEN SGFET had a lower carrier mobility (300 $cm^2\ V^{-1}\ s^{-1}$) than the SiO_2/Si SGFET (1250 $cm^2\ V^{-1}\ s^{-1}$) and this difference was ascribed to the higher scattering in PEN than in SiO_2 because of the higher root mean square (RMS) surface roughness (~5–10 nm for PEN and ~0.4–0.5 nm for SiO_2). Nevertheless, since the sensitivities were almost equal, the authors concluded that the substrate does not influence the pH response. The

PEN SGFET showed a good reversibility over repeated pH measurement cycles (decreasing and increasing ramps), but hysteresis was present. Mailly-Giacchetti *et al.* also studied the effect of the surface transfer doping due to the exchange of electrons between the adsorbed ions and graphene. The electron transfer reaction rate of graphene was reduced by fabricating an SGFETs on octadecyltrichlorosilane (OTS), as described in (ref. 54). The OTS-SGET sensitivity was 18 mV/pH, comparable with those of SiO_2/Si and PEN SGFETs, thus suggesting a negligible surface transfer doping.

Solid gate and three dimensional FETs

SGFETs are characterized via a direct application of V_G to the electrolyte solution, which is the gate dielectric. However, as a consequence any variability of the solution can affect the sensor response. The fabrication of a solid gate onto the SiO_2 substrate with a dielectric layer sandwiched between this gate and the graphene channel (Fig. 2a) is another FET configuration that improves the integration and microfabrication, as no cumbersome gate electrode (compared with the transistor dimensions) is needed.

Zhu *et al.* proposed a solid gate FET with HfO_2 as dielectric for pH sensing[55]. For a FET, the transconductance $g_m = \frac{\partial I_{DS}}{\partial V_G}$ expresses the sensitivity and is directly proportional to the capacitance of the dielectric (C_{ox}). Since HfO_2 is a high-dielectric constant material ($k \approx 25$), a high capacitance (i.e. $C_{ox}(HfO_2) = k\frac{\varepsilon_o}{t_{ox}} \approx 1.1$ μF/cm^2) is obtained for a thickness (t_{ox}) of just 20 nm. The choice of a high-k gate dielectric allows the thickness of the dielectric and the leakage current to be reduced, thus improving sensitivity. With a V_G from 0.6 to 1.6 V, this solid gate FET had a sensitivity of about 57.5 mV/pH in the pH interval 5.3–9.3 and a

359 V_{Dirac} positively shifting at increasing pH. The FET was tested at V_G = 0.75 V for real-time
360 sensing, but no information on repeatability and hysteresis was reported.
361 A further possible improvement to the FET configuration is the adoption of a 3D graphene
362 channel to enhance the transistor performances and reduce the power consumption[56,57]. A
363 graphene foam, i.e. a 3D network of single and double layer graphene, was grown on copper
364 and then transferred onto a glass substrate. Although the foam shrank after etching the
365 copper, the 3D structure was preserved. The Ti/Au source and drain had a contact
366 resistance of about 600 Ω/□, a high value probably due to the non-uniform shrinkage of the
367 foam. The top side of the graphene foam was coated with a layer of 20 nm of HfO_2 that was
368 in contact with an electrolyte solution. The length and width of the transistor were 0.6 and 5
369 mm, respectively. With a $V_G \in$ [-1.5, 1.5] V, the leakage current was about 3 orders of
370 magnitude lower than I_{DS}. Figure 2b shows the 3D graphene FET. The pH response was
371 tested in the range [3, 9] and the sensitivity was 79 ± 7 mV/pH. The authors attributed this
372 super-Nernstian sensitivity to the combination of 3D graphene foam and HfO_2, but this result
373 should be further investigated. The real-time monitoring was verified with a single
374 measurement at V_S = -0.5 V and V_{DS} = 0.5 V for pH decreasing from 9 to 3. Repeatability
375 and hysteresis were not reported.
376
377
378
379 **Graphene quantum dots**
380
381 Graphene quantum dots (GQDs) are low toxicity and high surface area particles with
382 diameters below 100 nm, typically between 3 and 20 nm. GQDs show quantum confinement
383 effects and a non-zero bandgap that can be tuned during preparation to modify the
384 photoluminescence (PL). The absorption spectra have a characteristic peak at about 230

nm and a typical PL quantum yield lower than approximately 30%. Their luminescence properties can be improved by new fabrication methods (e.g. water-phase molecular fusion and hydrothermal methods), doping or functionalization with organic, polymeric, inorganic, or biological molecules[58-63].

Although GQDs have only recently begun to show their potential for sensing applications, they have already been used in imaging of living cells, as probes for single-stranded deoxyribonucleic acid (ssDNA), detection of human immunoglobulin (IgG), adenosine triphosphate (ATP), thiols, and cleavage of DNA. Furthermore, the chemical synthesis of GQDs introduces oxygen-containing groups, e.g. carboxylic acid groups, and defects at the edges and in the basal plane, which make GQDs a promising material for pH sensing[64-68].

Huang et al. reported a wide PL emission range, from ultraviolet C to blue, for a GQD diameter between 1 and 2 nm, whereas a PL red shift and a decreasing band gap were observed for larger diameters. Furthermore, a blue shift was observed when pH moved from basic to acidic, and this was ascribed to the moving up of the exciton energy level. The authors suggested that the optical excitation could induce two kinds of excitons, i.e. within the whole GQD or in the edge microstructure. At decreased pH values, the passivation of the edge microstructure was responsible for the blue shift, whereas the wide emission spectra for small diameter size depended on the strong quantum confinement due to the excitons confined within the GQD[69].

Wu *et al.* synthesized nitrogen-doped GQDs (N-GQDs) using citric acid (CA) and dicyandiamide (DCD) as the carbon and nitrogen sources, respectively[70]. The N-GQDs were 1-2 graphene layers thick with an average diameter of 2.3 nm. The Fourier transform infrared spectroscopy (FTIR) and the XPS showed the presence of –COOH, –OH and $–NH_2$ groups. In buffer solutions from pH 2 to 9 and at an excitation wavelength λ_{ex}= 365 nm, the fluorescence intensity of N-GQDs was linearly proportional to pH and reversible during multiple cycles between pH 2 and 9. The zeta potential versus pH showed that these N-

GQDs are positively charged for pH < 2.7 and negatively charged for higher values (sensitivity ~ -4 mV/pH), which is a similar behaviour to that of amino acids. These N-GQDs were also used to measure the pH of river water, rain and tap water and gave comparable results with those of a commercial pH-meter. The biocompatibility was assessed with human epidermoid cancer cell lines (Hep-2) at an N-GQDs concentration of 1 $mg \cdot mL^{-1}$ for 24 h. The N-GQDs did not significantly alter the viability of cells and were permeable to cells membranes with an increasing fluorescence intensity from pH 5.7 to 8.

One year later, in 2015, Shi *et al.* used 3,4-dihydroxy-L-phenylalanine(L-DOPA) as the nitrogen source and the acronym N-OGQDs to stress that these GQDs were rich in oxygen atoms[71]. Their material had an average diameter of 12.5 nm and contained 66.58 wt% C, 4.01 wt% N, 5.77 wt% H, and 23.64 wt% O. The N-OGQDs were stable in high-ionic strength buffers (concentration of NaCl up to 1 M) and the PL intensity linearly increased in the pH range [3, 8] (λ_{ex} = 346 nm). Given the fluorescence intensity in arbitrary units (a.u.), the sensitivity was ≈ 80 a.u./pH. As for (ref. 61), the pH sensitivity can be ascribed to the reactivity of the amide and carboxylic groups. Although the N-OGQDs seemed potentially suitable for measuring pH in the physiological range, further tests are needed to evaluate parameters such as repeatability and accuracy.

Another synthetic approach for GQDs entailed the electrolysis of a graphite rod in a 5 mL dimethylsulfoxide (DMSO) solution with 0.01 M tetrabutylammonium perchlorate (TBAP)[72]. Yuan *et al.* obtained GQDs that consisted of approximately 1-3 graphene layers with an average diameter of about 10.6 nm. Sensitivity to pH was demonstrated in a wide range, i.e. [1, 14], with a particular behaviour at pH > 11. From 1 to 11, the PL intensity peak shifted from 522 to 575 nm due to the deprotonation of the functional groups, e.g. –COOH and –OH, which is in common with most previous pH sensors. However, from pH 12 to 14, the PL had new absorption peaks at 520-560 nm and a strong red emission centred at about 625 nm. The emission at 625 nm was stable even when the excitation wavelengths were

changed from 360 to 560 nm. The FTIR and XPS spectra showed the presence of a lactone structure that aroused by the tertiary alcohols reacting with nearby carboxylic acids at the edges of GQDs. In strong basic pH conditions, Yuan *et al.* verified that the lactone turned to quinone and caused the modification of the PL absorption spectra. In fact, when the GQDs were reduced by $NaBH_4$, which is known to eliminate lactone in graphene, there was a blue fluorescence instead of a red emission at basic pH and the solution colour turned to yellow instead of red at pH 13. From 1 to 13, the GQDs were pH-responsive from 10 up to 80°C and had a reversible fluorescence response over six consecutive heating-cooling cycles in this temperature range. The *in vivo* tests with human cervical cancer cells (HeLa) showed visible colour changes with a culture pH increasing from 5 to 9.

Park *et al.* grafted blue-emitting poly(7-(4-(acryloyloxy)butoxy)coumarin)-b-poly(N-isopropylacrylamide) (P7AC-b-PNIPAAm) to green-emitting 10 nm GQDs (block copolymer integrated GQDs, bcp-GQDs)[73]. At room temperature, the PL spectra of bcp-GQDs showed two emission peaks following an excitement at 365 nm, a first peak at 410 nm corresponding to the P7AC-b-PNIPAAm, and the other at 505 nm associated with the GQDs. The blue emission peak at 410 nm did not change with pH, whereas the green emission peak changed because of the protonation and deprotonation of the oxygen-based functional groups. However, the intensity ratio I_{510}/I_{410} plotted versus pH from 1 to 11 did not allow several pH values to be resolved, thus this promising idea should be further expanded with additional work in order to be of practical application.

Song *et al.* fabricated GQDs via a modified graphite intercalated compounds (GICs) method[74] and investigated the pH response[75]. Two GQDs diameters were investigated, i.e. GQD-A (2 ± 1 nm) and GQD-B (18 ± 2 nm), with an oxygen content of ~5 at% and ~8 at%, respectively. The FTIR spectra showed that the oxygen content was mostly due to the carboxyl groups and was lower than that of typical GQDs obtained from GO and rGO. In particular, GQD-A had a lower content than GQD-B. The carboxylic acid peak was absent

in GQD-A and much lower in GQD-B. Raman spectra indicated that these GQDs had a few defects and GQD-A had a stronger sp^2 hybridization than GQD-B. GQDs were tested with excitation wavelengths from 250 to 390 nm and at pH 2, 7 and 12. For GQD-A, the maximum PL intensity was at λ_{ex} = 315 nm at all pH values. The PL intensity decreased with increasing pH and the spectra were blue-shifted, sharper and with higher intensities at pH 2 than at pH 7 and 12, probably because of the protonation effect at basic pH on the edges and defect sites of GQD-A. Conversely, GQD-B had the lowest PL intensity at pH 2 and the maximum at pH 7 and 12 for λ_{ex} = 360 nm, with an increasing trend from basic to acidic pH.

The nanosheets synthesized by Joseph *et al.* were very close to nanodots, with average length and width of 135 and 137 nm, respectively, and a thickness of about 1-3 graphene layers[76]. These nanosheets were obtained by the aqueous exfoliation of graphite through the interaction with an antibacterial protein, the lysozyme (LYS). Since the isoelectric point (IEP) of LYS depends on the solution pH, the correlation between the LYS-nanosheets and the zeta potential was studied at different pHs from 1 to 13. The LYS-nanosheets IEP was about 8 with an initial pH of approximately 4. The zeta potential allowed the pH to be discriminated only between pH 1 and 5. At pH values below the IEP, the amines in the LYS-nanosheets led to a global positive charge that repelled the nanosheets from aggregations, whereas above the IEP the predominant effect was ascribed to the carboxylate ions that led to a global negative charge and a fine dispersion. On the other hand, around the IEP, the LYS-nanosheets aggregated because of a charge depletion. Interestingly, when tested for cytotoxicity with mouse embryonic fibroblasts (NIH-3T3) and three different cancer cells lines, namely human colorectal cancer cells (HCT-116), HeLa and squamous carcinoma cells (SCC-7), the LYS-nanosheets were less toxic for the NIH-3T3 than for the cancer cells. Although the cytotoxicity mechanism needs further investigation, these nanosheets showed promising properties for pH sensing.

Graphene oxide

Unlike graphene, GO is an electrical insulator due to its disrupted sp^2 bonding network, though there are several methods to restore the electrical conducitivity[77]. Although the precise chemical structure is still under investigation, the most widely accepted model was developed by Lerf and Klinowski[76] and describes GO as graphitic platelets characterized by epoxy and hydroxyl groups on the basal plane, and carboxyl groups on the edges. The large number of highly polar groups makes GO highly hydrophilic and a good candidate for measuring the pH of solutions. The pH dependence of GO in aqueous solutions has been investigated and the change in GO hydrophilicity has generally been ascribed to the protonation-deprotonation of the carboxyl groups[79–81]. At high pH, the hydrophilicity is enhanced and GO should behave like a surfactant, but since the surface tension is weak, it dissolves in water like a regular salt. At low pH, the degree of deprotonation is low and GO forms suspended aggregates with a sandwich-like structure GO-water-GO surrounded by water molecules.

Wang *et al.* prepared a GO colloid using a modified Hummers method and studied the role of pH, adjusted with HCl solution and aqueous ammonia, in the formation of a hydrogel[82,83]. The GO colloid aggregated into a cylindrical hydrogel at pH ≤5 or ≥10, whereas a black dispersion was obtained otherwise. This result depended on i) the degree of dissociation of carboxyl groups, whose charge state controlled the attraction-repulsion of GO sheets, ii) the concentration of GO, and iii) the use of HCl and ammonia, which reduced the thickness of the electrical double layer of the GO sheets.

With another modified version of the Hummers method, Qin *et al.* synthesized and dispersed about 20-50 mg of GO in 1 mL of purified water to obtain a self-assembled GO hydrogel

without any pre-processing[84]. The average size of the GO nanosheets was about 500 nm, and the thickness was between 0.911 and 0.607 nm, respectively. The hydrogel was obtained with a minimum GO concentration of 30 mg/mL. The gel formation was pH-dependent and only occurred for acidic pH. The GO hydrogel was stable when the GO concentration exceeded 5 wt%, probably because the π – π stacking and the hydrophobic interactions inhibited the pH-response. The ionization of the carboxyl groups, which increases with pH and reduces the number of the hydrogen bonds, was also exploited in hydrogels consisting of GO and poly(N-isopropylacrylamide), or GO and starch-based superabsorbent nanocomposites (SANCs), i.e. magnetic iron oxide nanoparticles and starch-g-poly(acrylic acid-o-acrylamide)[85,86].

Because of its insulator-like behaviour, the use of GO as pH sensor is generally associated with optical analysis. Lv *et al.* ultra-sonicated 2 mg/mL GO for 2 h to obtain GO hydrosols whose pH was adjusted from 2 to 11 with HCl or KOH aqueous solution[87]. Outside the pH range [2, 11], the hydrosol became unstable. After the centrifugation to remove the residual nanosheets, the GO hydrosols were heated in a water-thermal bath at about 85 °C for 30-45 min and formed thin membranes at the liquid/air interface. These GO membranes (GOMs) had a thickness of between 1.5 and 2 μm at pH 11 and 2, respectively. According to the ultraviolet-visible (UV-vis) spectra, the highest optical transmittance at 600 nm was about 30% at pH 2, and non-linearly decreased to about 1% at pH 11 (Fig. 3a). Lv *et al.* explained that this result was due to the deoxygenation of the GOMs in basic conditions, which led to a partial reduction of GO. The transmittance increased with increasing wavelength and was 65% at 1000 nm and pH 2. The transmittance of the GOMs at pH 2, 7 and 11 was also determined in the range [200, 3300] nm. Perhaps because of the presence of water molecules, the GOMs transmittances showed a non-linear dependence after 1300 nm, which can be thus assumed as the wavelength limit to use these GOMs as pH sensors.

Yan *et al.* proposed an optical pH sensor consisting of a film made up of polyethylenimine (PEI) functionalized lanthanide-doped ($NaYF_4$:Yb,Er) upconversion nanoparticles (PEI-UCNPs) and GO[88]. GO is a pH-dependent quencher for the luminescent PEI-UCNPs, and the fluorescent intensity can be used to sense pH. An amount of 0.5 mg/mL of PEI-UCNPs at pH 5 was mixed with 1 mg/mL GO and, after vacuum filtration and washing with water, a film was obtained leaving this dispersion to dry in air for two weeks. The GO-PEI-UCNPs film was dipped in buffer solutions and excited with a 980 nm laser. The fluorescence intensity at 540 nm linearly decreased (maximum 35%) when the pH changed in the physiological range from 5 to 8, with a response time of about 60 s for unitary changes of pH. The repeatability, stability and reversibility were demonstrated by cycling the film between pH 6 and 8 for five hours. This sensor was also tested with mice urine, which was diluted to obtain different pH conditions. The response was almost linear, with a maximum intensity shift of 55% between pH 4.95 and 8.05 (Fig. 3b). The GO-PEI-UCNPs film was found to be highly biocompatible *in vitro* when in contact with cultures of RAW264.7, MDA and MC3T3-E1 cell lines.

Chen *et al.* monitored the vis-near infrared (vis-NIR) fluorescence of GO to determine the changes in the extracellular pH during growth and metabolism of normal and cancer cells[89]. In buffer solutions, the fluorescence intensity at 650 nm of the single-layer GO nanosheets had a reversible sigmoidal response when the pH changed from 2 to 12 (Fig. 3c). The pH changes were also monitored in cultures of chronic granulocytic leukaemia (CGL) cancer cell (32D-BA) and normal mouse cells (32Dc-13). This test showed that the GO optical nanosheets were in linear correlation with a commercial pH meter ($R^2 = 0.99$) between pH 6.6 and 7.7.

In another work, PAA and poly(2-vinylpyridine) (P2VP) were grafted onto the surfaces of CdS/ZnS (blue emission at 440 nm) and CdSe/ZnS (orange emission at 580 nm) QDs, respectively. These two compounds were anchored to GO by π – π stacking interactions

566 between the pyrene groups of PAA and P2VP and the basal plane of GO. The GO-QDs (1
567 mg/mL) were characterized in aqueous media at different pH conditions with a λ_{ex} of 365
568 nm. The PL intensity of the blue peak was almost stable from pH 1 to 4, and increased from
569 pH 4 to 7. On the other hand, the PL intensity of the orange peak decreased from pH 1 to 5,
570 and saturated after pH 5. This effect could be explained by the fact that for pH < pKa = 3 the
571 P2VP chains swelled (P2VP-QDs size increased from ~45 to ~85 nm), whereas the PAA
572 chains swelled for pH > pKa = 4.5 (PAA-QDs size increased from ~30 to ~70 nm). The
573 swelling reduced the GO quenching and favoured the blue or the orange emission
574 depending on the pH value. The ratio of the two intensities, I_{580}/I_{440}, plotted versus pH from
575 1 to 7 showed a non-linear relationship that could be linearly approximated between pH 1
576 and 5 (sensitivity ~-0.56/pH, Fig. 3d). These GO-QDs were also reversible when cyclically
577 exposed to acid and basic pH[90].
578 A pH sensing material was obtained by combining DNA probes and GO in a work by Luo *et*
579 *al.*[91]. This sensor was fabricated by incubating DNA probes marked with the fluorescent dye
580 tetramethylrhodamine (TAMRA, 100 nM) in 20 µL phosphate buffer at different pH values
581 for 5 minutes, then adding ultra-pure water (68 µL) and GO (12 µL, concentration 100
582 µg/mL). Two DNA probes were designed to have different contents of the protein Tat, 50%
583 (probe 1) and 80% (probe 2). Tat allowed the DNA conformation to change at different pH
584 values, whereas the fluorescence signal of TAMRA was independent of pH. At basic pH,
585 the DNA probes had a hairpin structure with single stranded tails and were absorbed onto
586 the GO surface, thus the fluorescence was quenched. At acidic pH, the DNA probes
587 assumed a triplex structure, which is more rigid than the single stranded tail conformation.
588 In this case, the probes were not absorbed, and the fluorescence was not quenched. The
589 different Tat contents made the probes change the conformation at different pHs, thus
590 enabling the different pH values to be sensed. For pH < 5, probe 1 had a weak fluorescence
591 intensity and increased from pH 5 to 7. For pH > 7, the intensity saturated. Probe 2 had a

592 similar behaviour with a dynamic range between pH 6 and 8. Therefore, a combination of
593 probes 1 and 2 could be used to measure pH from 5 to 8.
594 Melai *et al.* presented an electrochemical GO pH sensor with a gold three-electrode screen
595 printed set-up. The working electrode (WE) was coated by a 400 nm GO layer and the
596 reference electrode (RE) was Ag/AgCl (the counter electrode was short-circuited to RE)[92].
597 The open-circuit circuit potential between WE and RE was linearly related to pH (range [4,
598 10]) in buffer solutions, with a sensitivity of about 32 mV/pH. This sensor was intended to
599 monitor wound pH, and measured values only differed less than 0.1 pH unit from those from
600 a commercial pH meter over a 4-day test in human exudate, i.e. a fluid mainly produced in
601 the inflammatory and proliferative phases of a wound[93].
602 Salvo *et al.* expanded the previous work and used a GO dispersion (4 mg/mL) to fabricate
603 a pH responsive film in the range [5, 9]. The resulting sensor (sensitivity ~43 mV/pH,
604 repeatability 0.2 pH unit and high linearity $R^2 = 0.99$) performed comparably to a commercial
605 pH meter (error = 0.14 ± 0.09 pH units) when tested in human plasma over one month[94].
606
607
608

609 ## Reduced graphene oxide

610
611 Like for GO, the literature reports several attempts to produce pH-sensitive rGO-based
612 dispersions. Liu *et al.* proposed pyrene-terminated poly(2-N-(dimethyl amino ethyl acrylate)
613 (PDMAEA) and PAA for polymer-rGO composites, but the pH-dependence of rGO was
614 negligible[95]. In another paper, after the synthesis of GO by a modified Hummers method,
615 Yang *et al.* added 10 mg of lysozyme from hen egg white to 20 mL of a GO solution before
616 reduction with 1 mL of hydrazine hydrate. After heating, ultra-sonication and centrifugation,
617 a lysozyme-rGO (lys-rGO) solution was obtained. The lysozymes adsorbed on GO, probably

618 due to π-π stacking and electrostatic interactions. They then acted as a dispersant, leading
619 to a low folding degree and flat lys-rGO with a higher carbon-oxygen (C/O) atomic ratio than
620 that of bare rGO. Furthermore, the lysozymes promoted the reduction of the oxygen-based
621 groups of GO, thus enhancing the restoration of the sp^2 hybridization, and stabilized the rGO
622 dispersion. The zeta-potential increased in absolute value when pH increased from 2.36 to
623 12.5, and were assumed to be linear between pH 4 and 10 (Fig. 4a)[96].
624 Liu *et al.* added chitosan to a GO solution before the reduction with hydrazine[97]. The zeta
625 potential was higher than 30 mV for 2 < pH < 5, probably because of the strong chitosan
626 protonation. After pH 5, the zeta potential rapidly decreased to about 9 mV at pH 6 and was
627 negative for pH ≥ 7 (Fig. 4b). This effect was probably due to the increased ionization of the
628 carboxylic groups in rGO and the decreased chitosan protonation. These effects led to the
629 aggregation of rGO at pH values higher than the pKa of chitosan (6.5) because the
630 electrostatic repulsive forces became too weak. The aggregation of rGO was highly
631 reversible when tested in repetitive cycles between pH 4 (dispersion) and 7 (aggregation).
632 The same behaviour was observed between pH 7 (aggregation) and 10 (dispersion). Ren
633 *et al.* described a polyacrylamide (PAM)–rGO composite that could be dispersed for pH ≥
634 4[98]. Although the PAM-rGO composite showed a pH dependence when characterized by
635 UV-vis, this optical analysis does not seem ready for pH sensing because the discrimination
636 between different pH values still needs improving.
637 Yang *et al.* treated GO with ozone before and after a thermal reduction process to obtain an
638 ozonized rGO quantum dots solution (O-rGO-QD)[99]. After the thermal reduction, the rGO
639 sheets were treated with ozone in water solution at pH 2 (O-rGO1) and 13 (O-rGO2), and
640 hydrothermally treated at pH < 1. Four other types of rGO sheets (O-rGO3 to O-rGO6) were
641 obtained after ozonation at pH 2, 7, 10 and 13, and a hydrothermal treatment at pH 13. After
642 drying, the O-rGOs were filtered through a microporous membrane to obtain a solution of
643 O–rGO quantum dots (O-rGO-QDx, x = 1..6, diameter 2-5 nm for x= 1 and 2, and 3-5 nm

644 for x = 3..6). The re-oxidation of GO through ozone formed carboxylic and ketone groups,
645 i.e. reactive sites for thermal reduction. These reactive sites were also introduced with the
646 ozone treatment after the reduction. The percentage of reactive sites depended on the pH
647 of the hydrothermal treatment, which increased the oxygen percentage from about 16% for
648 O-rGO-QD1 and O-rGO-QD 2 to a range of about [17, 27] % for O-rGO-QD3 up to O-rGO-
649 QD6. With an excitation wavelength of 254 nm, the fluorescence emission peak shifted
650 towards shorter wavelengths when pH increased from 2 to 13 during ozonation. Yang *et al.*
651 hypothesized that this phenomenon could be explained by the reaction of rGO with one of
652 the two forms of ozone in acid–base aqueous solution, i.e. dissolved ozone or $HO^{\cdot}$ radicals.
653 In acidic solution, the dissolved ozone is more reactive than the $HO^{\cdot}$ radicals, whereas the
654 opposite happens at basic pH. The O-rGO-QD1 fluorescence emission peak at 404 nm
655 reversibly increased for pH from 1 to 13 pH, with a negligible change in shape of the intensity
656 curve and a strong variation for pH > 7. The authors suggested several theories that could
657 explain this result, such as the triplet ground state[100] and the islets theories[101].
658 Srinives *et al.* fabricated an rGO pH sensor using L-ascorbic acid (L–AA) as the reducing
659 agent[102]. An rGO layer of unknown thickness and size bridging two electrodes (the
660 electrodes distance is not reported) was used to fabricate a chemiresistive sensor. The
661 normalized resistance ($\Delta R/R_0$) to the rGO resistance in air (R_0 ~6.7 KΩ) decreased for
662 unitary changes of pH from 3 to 8 with a sensitivity of 0.5 pH^{-1}, roughly. However, this study
663 does not seem mature enough for pH sensing as stability, repeatability, cycling tests and
664 large variations at low pH should be further characterized.
665 In 2013, Sohn *et al.* published the first paper on a solution-gated rGO FET for pH
666 detection[103]. The rGO FET had a SiO_2/Si substrate and the SiO_2 (100 nm thick) was exposed
667 to a 3% 3-aminopropyltriethoxysilane (APTES) aqueous solution. The APTES positively
668 charged SiO_2 with amino functional groups, so that the aggregation of GO nanosheets was
669 prevented when a GO solution was dropped on the substrate (nanosheet thickness ~1 nm,

diameter 0.5–1.5 mm). The rGO channel (resistance ~10–20 KΩ) between source and drain (length 400 mm, ratio width/length = 20) was obtained by reducing GO with hydrazine. The V_G was applied through an Ag/AgCl electrode in the range [-0.2, 0.2] V and constant V_{DS} = 0.1 V. The device had a $V_{Dirac} \cong 0 \pm 0.01$ V at pH 7 and low rGO carrier mobility (0.5 $cm^2/(V \cdot s)$) due to the residual –OH and –COOH functional groups on the rGO surface after reduction. The rGO FET was tested from pH 6 to 9 with unitary increments. The response was almost linear ($R^2 \cong 0.98$) with a sensitivity, i.e. $\Delta V_{Dirac}/\Delta pH$, of about 29 mV/pH. The reversibility seems good from the reported plot, but no numerical error was given. The repeatability error increased for increasing pH, with a maximum of about 20 mV at pH 9, i.e. almost one pH unit. The pH values from 9 to 6.11 were correctly discriminated when the rGO FET was tested during real-time measurements at constant V_G = -0.2 V. Unlike graphene, the rGO has oxygen functional groups in its structure, thus it is reasonable to assume that the modulation of the reduction process could improve the FET performances. Li *et al.* started with a SiO_2/Si substrate anisotropically etched to obtain reverse pyramids (35 µm deep, pitch distances 18, 35, 70, 105 and 140 µm) in Si (Fig. 4c)[104,105]. After spraying a commercial rGO solution onto the substrate and heating at 120 °C, the rGO was annealed in nitrogen at 300 °C for 1h and treated with oxygen plasma for 1 min. The sensing window was 4 x 4 mm^2 per sample. Transmission electron microscopy (TEM) and XPS analyses showed that the oxygen-plasma-treated (OPT)–rGO FET had more oxygen functional groups than the rGO FET. In terms of pH sensitivity, at $V_G \in [0, 4]$ V and V_{DS} = 0.2 V, the OPT-rGO FET (sensitivity ~53 mV/pH) performed better than the rGO FET on planar Si (45 mV/pH), whereas the OPT-rGO FET with the reverse-pyramid structure (RP-OPT-rGO FET) was even better (57.5 mV/pH for a pitch/depth ratio of 0.5) with high linearity (R^2 = 0.996) because of the increased sensing surface. The optimal power for oxygen plasma treatment was 20 W, since a decrease in sensitivity was observed at higher values. Hysteresis, defined as the voltage offset between the beginning and the end of the test, was calculated for the

pH loop sequence 7, 3, 7, 11 and 7. For rGO, OPT-rGO and RP-OPT-rGO FETs, the offsets were about 19, 13, and 11 mV, respectively. Therefore, the RP-OPT-rGO FET outperformed the other configurations.

Conclusions and outlook

Developing a graphene-based pH sensor is challenging. Although graphene-based materials have pH-dependent electrochemical properties, current pH sensors are not sufficiently advanced for new products to enter the market.

In this review, the field effect transistor was the most used pH-sensing architecture. Table 2 summarizes the efforts reported in the literature to create a graphene-based pH sensor. Most FETs adopt graphene as the conduction channel, whereas there are only two examples of rGO FETs. The sensitivity of these devices ranges from about 6 to 99 mV/pH and such a wide spectrum suggests that researchers are still looking for an optimum solution. Pristine graphene is scarcely sensitive to pH, but defects such as oxygenated functional groups can modify its chemical structure and turn it into a pH-sensitive material that can rival other existing pH sensors.

However, a standard fabrication process is not yet available and small differences can lead to large variations. The control of defects is of primary importance to obtain reliable pH sensors, especially the amount of –COOH groups at the graphene edges. It has been demonstrated that oxygen plasma treatment or anodization can increase the number of reactive sites to H^+ and OH^- ions. Another improvement could be the increase in the pH sensitive area, as some solutions with suspended and 3D graphene have demonstrated.

These approaches can pave the way towards a standardized fabrication technology, but they are only one side of the whole picture. Unfortunately, the pH response can be affected

by impurities and residual resist such as silanol and silylamine groups that modify the net charge of the substrate surface, typically SiO_2 on Si. This problem could be solved by improving the manufacturing techniques, but the effect of interfering ions such as Na^+, Cl^- and K^+ could still be a serious limiting factor.

This review has presented proof-of-concept pH sensors usually tested in reference buffer solutions. However, some works showed that the pH response changes when electrolytes are added to the buffer solutions. This could limit the applicability of these sensors in real case studies. Quantum dots based on graphene, GO and rGO are an emerging alternative to FETs to bridge the performance gap between the FETs and pH sensing (Table 3). For example, the GQDs described in ref. 63 were successfully tested in river, rain and tap water, and passed the biocompatibility tests. However, GQDs are still confined to lab research because of limitations, such as the difficulty to achieve large scale production and high quantum yield, and to understand correctly the quantum confinement and the doping mode (e.g. lattice and edge modes)[69,106,107].

The future of graphene-based pH sensors will probably be decided by the ability of researchers to produce effective results with FETs and GQDs. Although they can be combined with other pH-sensitive materials, graphene, GO and rGO are likely to have a considerable impact on pH sensing as stand-alone pH sensitive materials and this entails a deeper understanding of the chemical interactions with hydrogen ions.

Acknowledgements

This work was partially supported from the European Commission through the SWAN-iCare project (FP7-ICT-317894).

Author contributions

P.S. conceived and wrote the paper. P.S., B.M., N.C. and C.P. were responsible of the graphene and graphene oxide sections. P.S., A.K. and F.B. were responsible of the reduced graphene oxide section. M.G.T. and R.F. were responsible of pH chemistry throughout the paper. F.D.F. supervised and edited the paper.

Competing financial interests

The authors declare no competing financial interests.

References

1. Kurkdjian, A., Guern, J. Intracellular pH: Measurement and Importance in Cell Activity. *Annu. Rev. Plant Biol.* **40**, 271–303 (1989).
2. Slonczewski, J. L., Fujisawa, M., Dopson, M., Krulwich, T. A. Cytoplasmic pH measurement and homeostasis in bacteria and archaea. *Adv. Microb. Physiol.* **55**, 1–79 (2009).
3. Forstner, U., Wittmann, G. T. W. *Metal Pollution in the Aquatic Environment*, 2nd Ed., (Springer, 1983).
4. Harter, R. D. Effect of Soil pH on Adsorption of Lead, Copper, Zinc, and Nickel. *Soil. Sci. Soc. Am. J.* **47**, 47–51 (1982).

5. Bohnke, Cl., Duroy, H., Fourquet, J.-L. pH sensors with lithium lanthanum titanate sensitive material: applications in food industry. *Sensor. Actuat. B-Chem.* **89**, 240–247 (2003).
6. Gillies, R. J., Raghunand, N., Garcia-Martin, M. L., Gatenby, R. A. pH imaging. A review of pH measurement methods and applications in cancers. *IEEE Eng. Med. Biol.* **23**, 57–64 (2004).
7. Zhao, C., Nie, S., Tang, M., Sun, S. Polymeric pH-sensitive membranes—A review. *Prog. Polym. Sci.* **36**, 1499–1520 (2011).
8. Korostynska, O., Arshak, K., Gill, E., Arshak, A. Review on State-of-the-art in Polymer Based pH Sensors. *Sensors (Basel)* **7**, 3027–3042 (2007).
9. Korostynska, O., Arshak, K., Gill, E., Arshak, A. Review Paper: Materials and Techniques for in Vivo pH Monitoring. *IEEE Sensors J.* **8**, 20-28 (2008).
10. Bizzarri, R., Serresi, M., Luin, S., Beltram, F. Green fluorescent protein based pH indicators for in vivo use: a review. *Anal. Bioanal. Chem.* **393**, 1107–1122 (2009).
11. Richter, A. *et al.* Review on Hydrogel-based pH Sensors and Microsensors. *Sensors (Basel)* **8**, 561–581 (2008).
12. Sheppard, N.F. Jr., Lesho, M. J., McNally, P., Shaun Francomacaro, A. Microfabricated conductimetric pH sensor. *Sensor. Actuat. B-Chem.* **28**, 95–102 (1995).
13. Baldini, F. Critical review of pH sensing with optical fibres Chemical, Biochemical, and Environmental Fiber Sensors X. *Proc. SPIE* **3540**, 2–9 (1998).
14. Vonau, W., Guth, V. pH Monitoring: a review. *J. Solid State Electrochem.* **10**, 746–752 (2006).
15. Sandifer, J. R., Voycheck, J. J. A Review of Biosensor and Industrial Applications of pH-ISFETs and an Evaluation of Honeywell's "DuraFET". *Mikrochim. Acta* **131**, 91–98 (1999).

16. Zuliani, C., Matzeu, G., Diamond, D. A potentiometric disposable sensor strip for measuring pH in saliva. *Electrochim. Acta* **132**, 292–296 (2014).
17. Shiu, K.-K., Song, F., Dai, H.-P. Potentiometric pH sensor with anthraquinonesulfonate adsorbed on glassy carbon electrodes. *Electroanal.* **8**, 1160–1164 (1996).
18. Thompson, B. C., Winther-Jensen, O., Winther-Jensen, B., MacFarlane, D. R. A solid-state pH sensor for nonaqueous media including ionic liquids. *Anal. Chem.* **85**, 3521–5 (2013).
19. Guinovart, T., Valdés-Ramírez, G., Windmiller, J. R., Andrade, F. J., Wang, J. Bandage-Based Wearable Potentiometric Sensor for Monitoring Wound pH. *Electroanal.* **26**, 1345–1353 (2014).
20. Tian, M., Peng, X., Fan, J., Wang, J., Sun, S. A fluorescent sensor for pH based on rhodamine fluorophore. *Dyes Pigments* **95**, 112–115 (2012).
21. Shi, W., Li, X., Ma, H. A tunable ratiometric pH sensor based on carbon nanodots for the quantitative measurement of the intracellular pH of whole cells. *Angew. Chem. Int. Ed. Engl.* **51**, 6432–6435 (2012).
22. Schyrr, B. *et al.* Development of a polymer optical fiber pH sensor for on-body monitoring application. *Sensor. Actuat. B-Chem.* **194**, 238–248 (2014).
23. Schreml, S. *et al.* A sprayable luminescent pH sensor and its use for wound imaging in vivo. *Exp. Dermatol.* **21**, 951–953 (2012).
24. Ahn, J.-H. *et al.* A pH sensor with a double-gate silicon nanowire field-effect transistor. *Appl. Phys. Lett.* **102**, 083701 (2013).
25. Duroux, P. *et al.* The ion sensitive field effect transistor (ISFET) pH electrode: a new sensor for long term ambulatory pH monitoring. *Gut* **32**, 240–245 (1991).

26. Chen, Y., Wang, X., Erramilli, S., Mohanty, P., Kalinowski, A. Silicon-based nanoelectronic field-effect pH sensor with local gate control. *Appl. Phys. Lett.* **89**, 223512 (2006).
27. Das, A. *et al.* Highly sensitive palladium oxide thin film extended gate FETs as pH sensor. *Sensor. Actuat. B-Chem.* **205**, 199–205 (2014).
28. Sandifer, J. R., Voycheck, J. J. A Review of Biosensor and Industrial Applications of pH-ISFETs and an Evaluation of Honeywell's "DuraFET". *Mikrochim. Acta* **131**, 91–98 (1999).
29. Geim, A. K., Novoselov, K. S. The rise of graphene. *Nat. Mater.* **6**, 183–191 (2007).
30. Pumera, M. Electrochemistry of graphene: new horizons for sensing and energy storage. *Chem. Rec.* **9**, 211–223 (2009).
31. Brownson, D. A. C., Banks, C. E. Graphene electrochemistry: an overview of potential applications. *Analyst.* **135**, 2768–2778 (2010).
32. *Nature Mat.* **15**, 485 (2016).
33. Feng, L., Liu, Z. Graphene in Biomedicine: Opportunities and Challenges. *Nanomedicine*. **6**, 317–324 (2011).
34. Zhu, Y. *et al.* Graphene and Graphene Oxide: Synthesis, Properties, and Applications. *Adv. Mater.* **22**, 3906–3924 (2010).
35. Abdolhosseinzadeh, S., Asgharzadeh, H., Kim, H. S. Fast and fully-scalable synthesis of reduced graphene oxide. *Sci. Rep.* **5**, 10160 (2015).
36. Ang, P. K., Chen, W., Wee, A.T., Loh, K. P. Solution-gated epitaxial graphene as pH sensor. *J. Am. Chem. Soc.* **130**, 14392–14393 (2008).
37. Lei, N., Li, P., Xue, W., Xu, J. Simple graphene chemiresistors as pH sensors: fabrication and characterization. *Meas. Sci. Technol.* **22**, 107002 (2011).

38. Lee, C-Y., Lei, K. F., Tsai, S-W., Tsang, N-M. Development of Graphene-based Sensors on Paper Substrate for the Measurement of pH Value of Analyte. *BioChip J.* DOI 10.1007/s13206-016-0304-7, 1–7 (2016).
39. Ohno, Y., Maehashi, K., Yamashiro, Y., Matsumoto, K. Electrolyte-gated graphene field-effect transistors for detecting pH and protein adsorption. *Nano Lett.* **9**, 3318–3322 (2009).
40. Ristein, J. Characteristics of solution gated field effect transistors on the basis of epitaxial graphene on silicon carbide. *J. Phys. D: Appl. Phys.* **43**, 345303 (2010).
41. Cheng, Z., Li, Q., Li, Z., Zhou, Q., Fang, Y. Suspended Graphene Sensors with Improved Signal and Reduced Noise. *Nano Lett.* **10**, 1864–1868 (2010).
42. Lee, M. H. *et al.* Apparent pH sensitivity of solution-gated graphene transistors. *Nanoscale* **7**, 7540–7544 (2015).
43. Heller, I. *et al.* Influence of Electrolyte Composition on Liquid-Gated Carbon Nanotube and Graphene Transistors. *J. Am. Chem. Soc.* **132**, 17149–17156 (2010).
44. Fu, W. *et al.* Graphene Transistors Are Insensitive to pH Changes in Solution. *Nano Lett.* **11**, 3597–3600 (2011).
45. Kwon, S. S. *et al.* Reversible and Irreversible Responses of Defect-Engineered Graphene-Based Electrolyte-Gated pH Sensors. *ACS Appl. Mater. Interfaces.* **8**, 834–839 (2016).
46. Tan, X., Chuang, H-J., Lin, M-W., Zhou, Z., Cheng, M. M-C. Edge Effects on the pH Response of Graphene Nanoribbon Field Effect Transistors. *J. Phys. Chem. C.* **117**, 27155–27160 (2013).
47. Zhang, B., Cui, T. Suspended Graphene Nanoribbon Ion-Sensitive Field-Effect Transistors Formed by Shrink Lithography for pH/Cancer Biomarker Sensing. *J. Microelectromech. Syst.* **22**, 1140–1146 (2013).

872 48. Lim, C. X., Hoh, H. Y., Ang, P. K., Loh, K. P. Direct Voltammetric Detection of DNA
873 and pH Sensing on Epitaxial Graphene: An Insight into the Role of Oxygenated
874 Defects. *Anal. Chem.* **82**, 7387–7393 (2010).
875 49. Bott, A. W. Electrochemistry of Semiconductors. *Curr. Sep.* **17**, 87–91 (1998).
876 50. Zaifuddin, N. M. *et al.* pH Sensor Based on Chemical-Vapor-Deposition-Synthesized
877 Graphene Transistor Array. *Jpn. J. Appl. Phys.* **52**, 06GK04, (2013).
878 51. Lin, X. *et al.* Graphene Channel Liquid Container Field Effect Transistor as pH
879 Sensor. *J. Nanomater.* **2014**, 547139 (2014)
880 52. Kiani, M. J. *et al.* Analytical modelling of monolayer graphene-based ion-sensitive
881 FET to pH changes. *Nanoscale Res. Lett.* **8**, 173–181 (2013).
882 53. Mailly-Giacchetti, B. *et al.* pH sensing properties of graphene solution-gated field-
883 effect transistors. *J. Appl. Phys.* **114**, 084505 (2013).
884 54. Wang, Q. H. *et al.* Understanding and controlling the substrate effect on graphene
885 electron-transfer chemistry via reactivity imprint lithography. *Nat. Chem.* **4**, 724–732
886 (2012).
887 55. Zhu, Y. *et al.* A solid-gated graphene FET sensor for pH measurements. *Proc. of the*
888 *IEEE International Conference on Micro Electro Mechanical Systems (MEMS) 2015*,
889 869–872 (2015).
890 56. Ameri, S. K., Singh, P. K., Sonkusale, S. R. Liquid gated three dimensional graphene
891 network transistor. *Carbon* **79**, 572–577 (2014).
892 57. Ameri, S. K., Singh, P. K., Sonkusale, S. R. Three Dimensional Monolayer Graphene
893 Foam for Ultra-Sensitive pH Sensing. *18th International Conference on Solid-State*
894 *Sensors, Actuators and Microsystems (TRANSDUCERS)*, 1378–1380 (2015).
895 58. Wang, Z., Zeng, H., Sun, L. Graphene quantum dots: versatile photoluminescence
896 for energy, biomedical, and environmental applications. *J. Mater. Chem. C*. **3**, 1157–
897 1165 (2015).

59. Du, Y., Guo, S. Chemically doped fluorescent carbon and graphene quantum dots for bioimaging, sensor, catalytic and photoelectronic applications. *Nanoscale*. **8**, 2532–43 (2016).

60. Li, X., Rui, M., Song, J., Shen, Z., Zeng, H. Carbon and Graphene Quantum Dots for Optoelectronic and Energy Devices: A Review. *Adv. Funct. Mater.* **25**, 4929–4947, (2015).

61. Sun, H., Wu, L., Wei, W., Qu, X. Recent advances in graphene quantum dots for sensing. *Mater. Today.* **16**, 433–442 (2013).

62. Wang, L. *et al.* Gram-scale synthesis of single-crystalline graphene quantum dots with superior optical properties. *Nat. Commun.* **5**, 5357 (2014).

63. Gu, J. *et al.* High-yield synthesis of graphene quantum dots with strong green photoluminescence. *RSC Adv.* **4**, 50141-50144 (2014).

64. Bacon, M., Bradley, S. J., Nann, T. Graphene Quantum Dots. *Part. Part. Syst. Charact.* **31**, 415–428 (2014).

65. Shen, J., Zhu, Y., Yang, X., li, C. Graphene quantum dots: emergent nanolights for bioimaging, sensors, catalysis and photovoltaic devices. *Chem. Commun.* **48**, 3686–3699 (2012).

66. Li, L. *et al.* Focusing on luminescent graphene quantum dots: current status and future perspectives. *Nanoscale* **5**, 4015–4039 (2013).

67. Liu, R., Wu, D., Feng, X., Müllen, K. Bottom-Up Fabrication of Photoluminescent Graphene Quantum Dots with Uniform Morphology. *J. Am. Chem. Soc.* **133**, 15221–15223 (2011).

68. Yang, F. *et al.* Influence of pH on the fluorescence properties of graphene quantum dots using ozonation pre-oxide hydrothermal synthesis. *J. Mater. Chem.* **22**, 25471–25479 (2012).

69. Huang *et al.* Anomalous Light Emission and Wide Photoluminescence Spectra in Graphene Quantum Dot: Quantum Confinement from Edge Microstructure. *J. Phys. Chem. Lett.* **7**, 2888–2892 (2016).
70. Wu., Z. L. *et al.* A general quantitative pH sensor developed with dicyandiamide N-doped high quantum yield graphene quantum dots. *Nanoscale* **6**, 3868–3874 (2014).
71. Shi, B. *et al.* One-pot green synthesis of oxygen-rich nitrogen-doped graphene quantum dots and their potential application in pH-sensitive photo-luminescence and detection of mercury(II) ions. *Talanta* **142**, 131–139 (2015).
72. Yuan, F. *et al.* Multicolor Fluorescent Graphene Quantum Dots Colorimetrically Responsive to All-pH and Wide Temperature Range. *Nanoscale* **7**, 11727–11733 (2015).
73. Park, C. H. *et al.* Multicolor Emitting Block Copolymer-Integrated Graphene Quantum Dots for Colorimetric, Simultaneous Sensing of Temperature, pH, and Metal Ions. *Chem. Mater.* **27**, 5288−5294 (2015).
74. Song, S.H. *et al.* Highly Efficient Light-Emitting Diode of Graphene Quantum Dots Fabricated from Graphite Intercalation Compounds. *Adv. Opt. Mater.* **2**, 1016–1023 (2014).
75. Song, S.H. *et al.* Size and pH dependent photoluminescence of graphene quantum dots with low oxygen content. *RSC Adv.* **6**, 97990-97994 (2016).
76. Joseph, D., Tyagi, N., Ghimire, A., Geckeler, K. E. A direct route towards preparing pH-sensitive graphene nanosheets with anti-cancer activity. *RSC Adv.* **4**, 4085–4093 (2014).
77. Stankovich, S. et al. Graphene-based composite materials. *Nature* **442**, 282–286 (2006).
78. Dreyer, D. R., Park, S., Bielawski, C. W., Ruoff, R. S. The chemistry of graphene oxide. *Chem. Soc. Rev.* **39**, 228–240 (2010).

79. Shih, C-J., Lin, S., Sharma, R., Strano, M. S., Blankschtein, D. Understanding the pH-Dependent Behavior of Graphene Oxide Aqueous Solutions: A Comparative Experimental and Molecular Dynamics Simulation Study. *Langmuir* **28**, 235–241 (2012).

80. Bai, H., Li, C., Wang, X. A pH-sensitive graphene oxide composite hydrogel. *Chem. Commun.* **46**, 2376–2378 (2010).

81. Hui, W. *et al.* pH-dependent size，surface chemistry and electrochemical properties of graphene oxide. New Carbon Mater. 28, 327–335 (2013).

82. Wang, G. *et al.* Self-assembled graphene monoliths: properties, structures and their pH-dependent self-assembly behavior. *New Carbon Mater.* **30**, 30–40 (2015).

83. Hummers, W. S. Jr., Offeman, R. E. Preparation of Graphitic Oxide. *J. Am. Chem. Soc.* **80**, 1339–1339 (1958).

84. Qin, S-Y., Liu, X-L., Zhuo, R-X., Zhang, X-Z. Microstructure-Controllable Graphene Oxide Hydrogel Film Based on a pH-Responsive Graphene Oxide Hydrogel. *Macromol. Chem. Phys.* **213**, 2044−2051 (2012).

85. Sun, S., Wu, P. A one-step strategy for thermal- and pH-responsive graphene oxide interpenetrating polymer hydrogel networks. *J. Mater. Chem.* **21**, 4095–4097 (2011).

86. Hosseinzadeh, H., Ramin, S. Magnetic and pH-responsive starch-g-poly(acrylic acid-co-acrylamide)/graphene oxide superabsorbent nanocomposites: One-pot synthesis, characterization, and swelling behavior. *Starch/Stärke* **68**, 200–212 (2016).

87. Lv, W. *et al.* pH-Mediated fine-tuning of optical properties of graphene oxide membranes. *Carbon* **50**, 3233−3239 (2012).

88. Yan, L. *et al.* Biocompatible and flexible graphene oxide/upconversion nanoparticle hybrid film for optical pH sensing. *Phys. Chem. Chem. Phys.* **16**, 1576−1582 (2014).

89. Chen, J-L., Yan, X-P. Ionic strength and pH reversible response of visible and near-infrared fluorescence of graphene oxide nanosheets for monitoring the extracellular pH. *Chem. Commun.* **47**, 3135–3137 (2011).

90. Paek, K., Yang, H., Lee, J., Park, J., Kim, B. J. Efficient Colorimetric pH Sensor Based on Responsive Polymer - Quantum Dot Integrated Graphene Oxide. *ACS Nano* **8**, 2848–2856 (2014).

91. Luo, F., Xi, Q., Jianhui, J., Yu, R. Graphene oxide based DNA nanoswitches as a programmable pH-responsive biosensor. *Anal. Methods.* **8**, 6982-6985 (2016).

92. Melai, B. *et al.* A graphene oxide pH sensor for wound monitoring. *Proc. of Engineering in Medicine and Biology Society (EMBC), 38th Annual International Conference of the IEEE*, 1898–1901 (2016).

93. Salvo, P., Dini, V., Di Francesco, F., Romanelli, M. The role of biomedical sensors in wound healing. *Wound Medicine* **8**, 15–18 (2015).

94. Salvo, P. *et al.* Temperature and pH sensitive wearable materials for monitoring foot ulcers. *Int. J. Nanomedicine.* accepted for publication, 2017.

95. Liu, J. *et al.* Synthesis, Characterization, and Multilayer Assembly of pH Sensitive Graphene-Polymer Nanocomposites. *Langmuir* **26**, 10068–10075 (2010).

96. Yang, F., Liu, Y., Gao, L., Sun, J. pH-Sensitive Highly Dispersed Reduced Graphene Oxide Solution Using Lysozyme via an in Situ Reduction Method. *J. Phys. Chem. C* **114**, 22085–22091 (2010).

97. Liu, J. *et al.* Multiple pH-responsive graphene composites by non-covalent modification with chitosan. *Talanta* **101**, 151–156 (2012).

98. Ren, L. *et al.* A smart pH responsive graphene/polyacrylamide complex via noncovalent interaction. *Nanotechnology* **21**, 335701–335706 (2010).

997 99. Yang, F. *et al.* Influence of pH on the fluorescence properties of graphene quantum
998 dots using ozonation pre-oxide hydrothermal synthesis. *J. Mater. Chem.* **22**, 25471–
999 25479 (2012).
1000 100. Pan, D., Zhang, J., Li, Z., Wu, M. Hydrothermal route for cutting graphene
1001 sheets into blue-luminescent graphene quantum dots. *Adv Mater.* **22,** 734–738
1002 (2010).
1003 101. Eda, G. *et al.* Blue Photoluminescence from Chemically Derived Graphene
1004 Oxide. *Adv. Mater.* **22**, 505–509 (2010).
1005 102. Srinives, S. *et al.* A development of a graphene based chemiresistive sensor:
1006 demonstrations on pH sensing, and cell detection. *Adv. Mat. Res.* **1103**, 137–143
1007 (2015).
1008 103. Sohn, I-Y. *et al.* pH sensing characteristics and biosensing application of
1009 solution-gated reduced graphene oxide field-effect transistors. *Biosens. Bioelectron.*
1010 **45**, 70–76 (2013).
1011 104. Li, Y-R. *et al.* Highly Sensitive pH Sensors of Extended-Gate Field-Effect
1012 Transistor With the Oxygen-Functionalized Reduced Graphene Oxide Films on
1013 Reverse Pyramid Substrates. *IEEE Electron. Device Lett.* **36**, 1189–1191 (2015).
1014 105. Li, Y-R. *et al.* High-sensitivity extended-gate field-effect transistors as pH
1015 sensors with oxygen-modified reduced graphene oxide films coated on different
1016 reverse-pyramid silicon structures as sensing heads. *Jpn. J. Appl. Phys.* **55**, 04EM08
1017 (2016).
1018 106. Sun, J. *et al.* Ultra-High Quantum Yield of Graphene Quantum Dots: Aromatic-
1019 Nitrogen Doping and Photoluminescence Mechanism. *Part. Part. Syst. Charact.* **32**,
1020 434–440 (2015).
1021 107. Jiang, D. *et al.* Synthesis of Luminescent Graphene Quantum Dots with High
1022 Quantum Yield and Their Toxicity Study. *PLoS One.* **10**, e0144906 (2015).

Figures

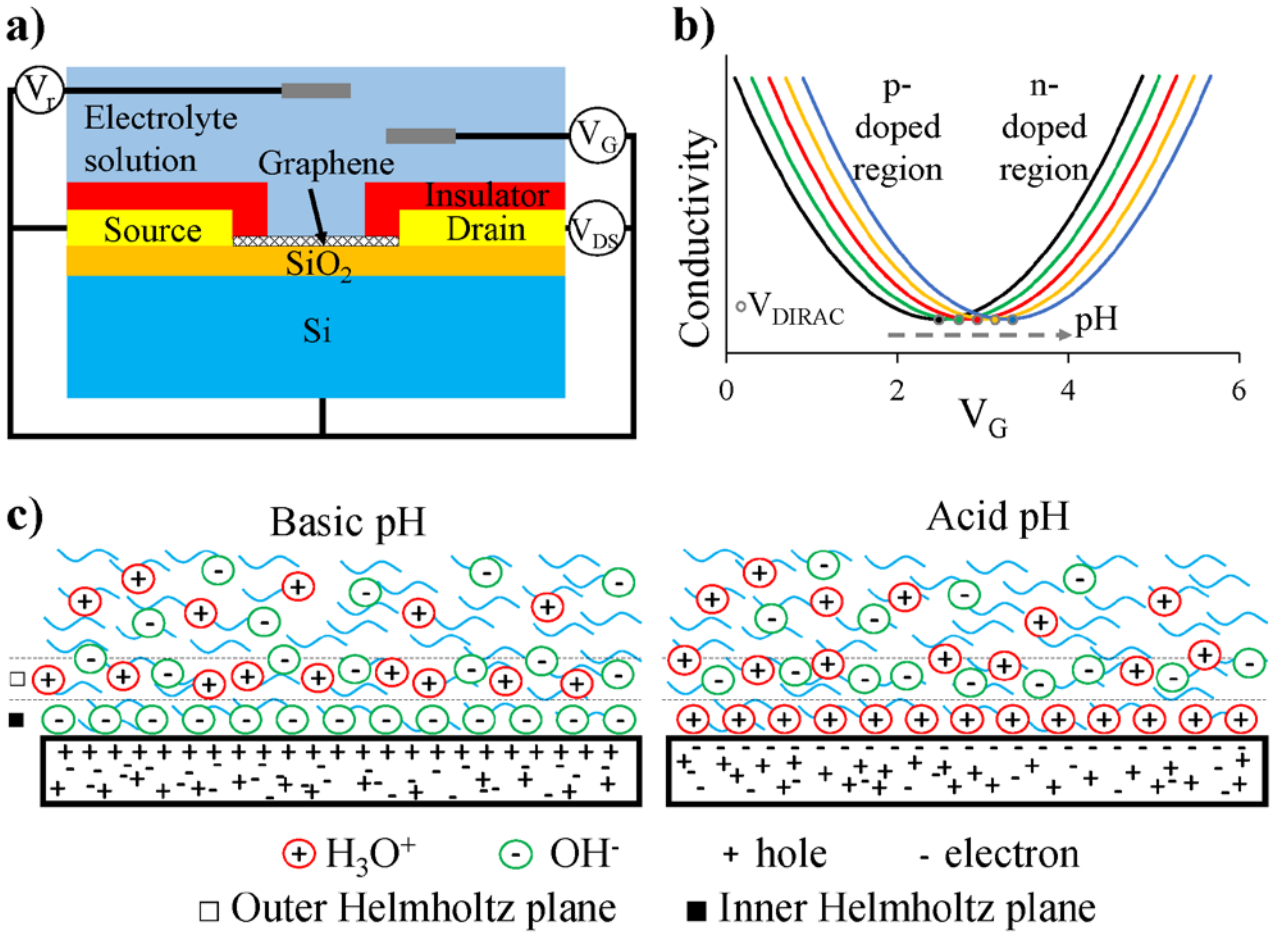

Figure 1. a) Three-electrode configuration of a pH-measuring FET. Although the most common configuration is with V_G applied through a Ag/AgCl reference electrode and no counter electrode, this ISFET provides the most accurate measurement; b) example of the V_{Dirac} shift when pH increases. The area to the left of V_{Dirac} is associated with an excess of holes in the graphene channel, and with an excess of electrons to the right. The determination of the V_{Dirac} allows the measurement of pH; c) Distribution of ions and donors (holes or electrons) at the graphene-electrolyte solution at basic and acid pH.

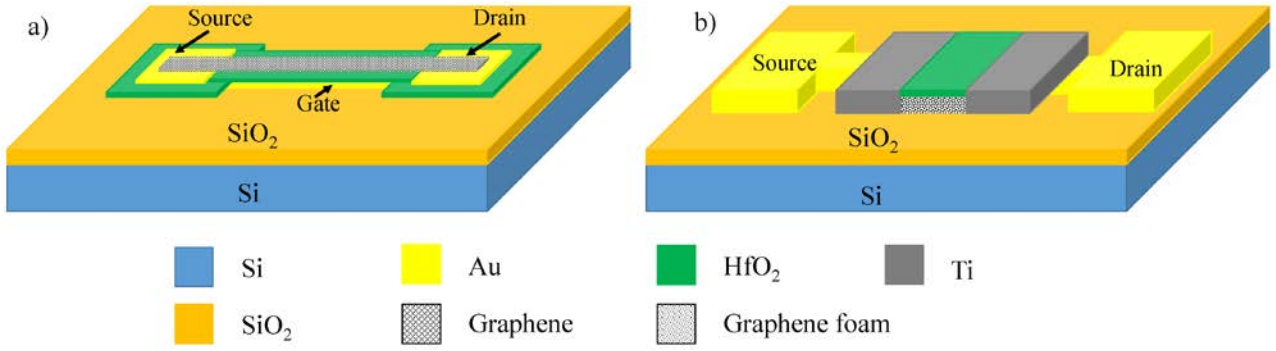

1034

1035 Figure 2. a) Field effect transistor with a solid gate under a HfO_2 layer; b) Three dimensional
1036 field effect transistor where a graphene foam coated with a 20 nm HfO_2 layer is the pH-
1037 sensitive material (modified from refs. 56 and 57).

1038

1039

1040

1041

1042

1043

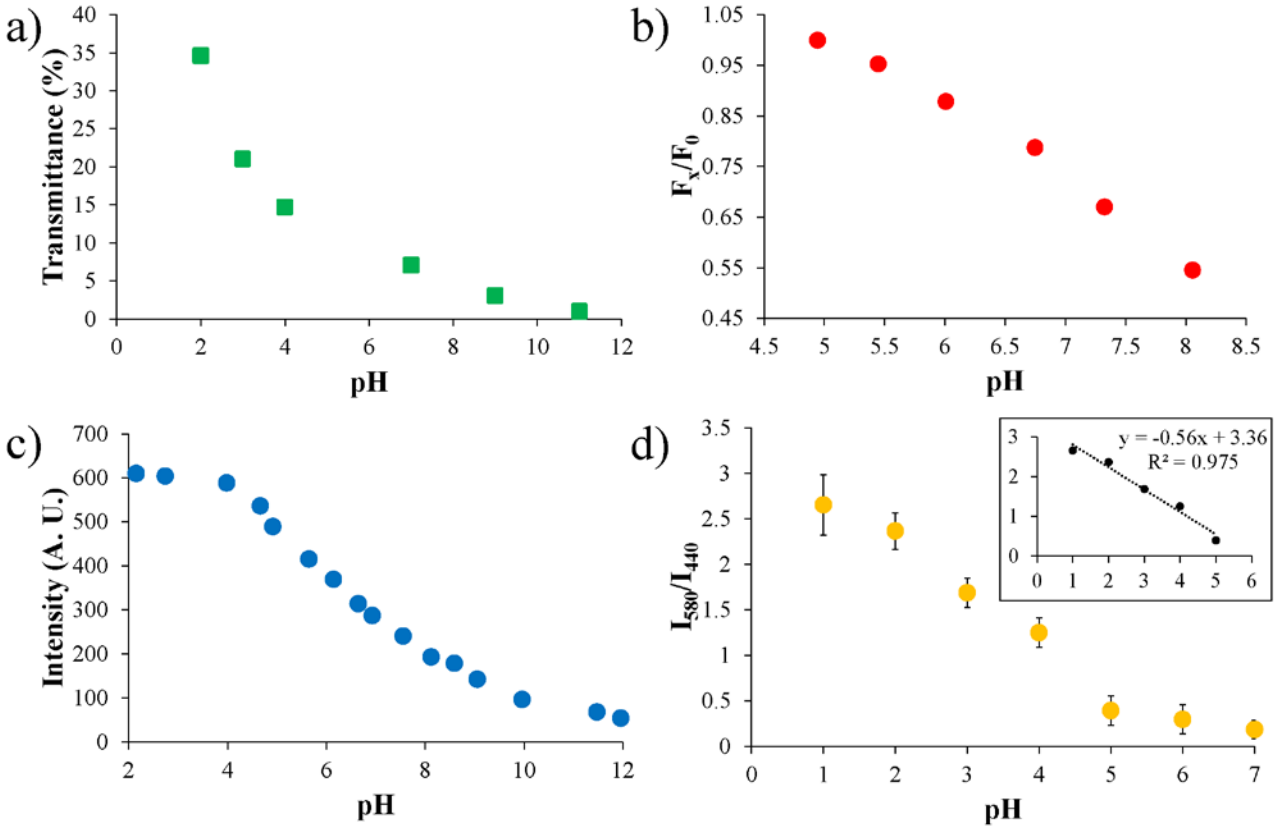

Figure 3. a) Optical transmittance of the GOMs at 600 nm. The decrease in transmittance depended on the deoxygenation and partial reduction of the GOMs in basic conditions (modified from ref. 87); b) Response of the GO-PEI-UCNPs in solutions of diluted mice urine. F_0 is the fluorescence intensity at 540 nm at pH 5, whereas F_x is the fluorescence intensity at the pH under test (modified from ref. 88); c) fluorescence intensity of the GO single-layer nanosheets at λ_{ex} of 650 nm. The intensity can be linearly approximated in the pH physiological range [4, 8] (modified from ref. 89); d) response of the PAA-P2VP-GO-QDs reported as the ratio between the orange (I_{580}) and the blue (I_{440}) emission intensities versus pH. Inset: linear approximation between pH 1 and 5 (modified from ref. 90).

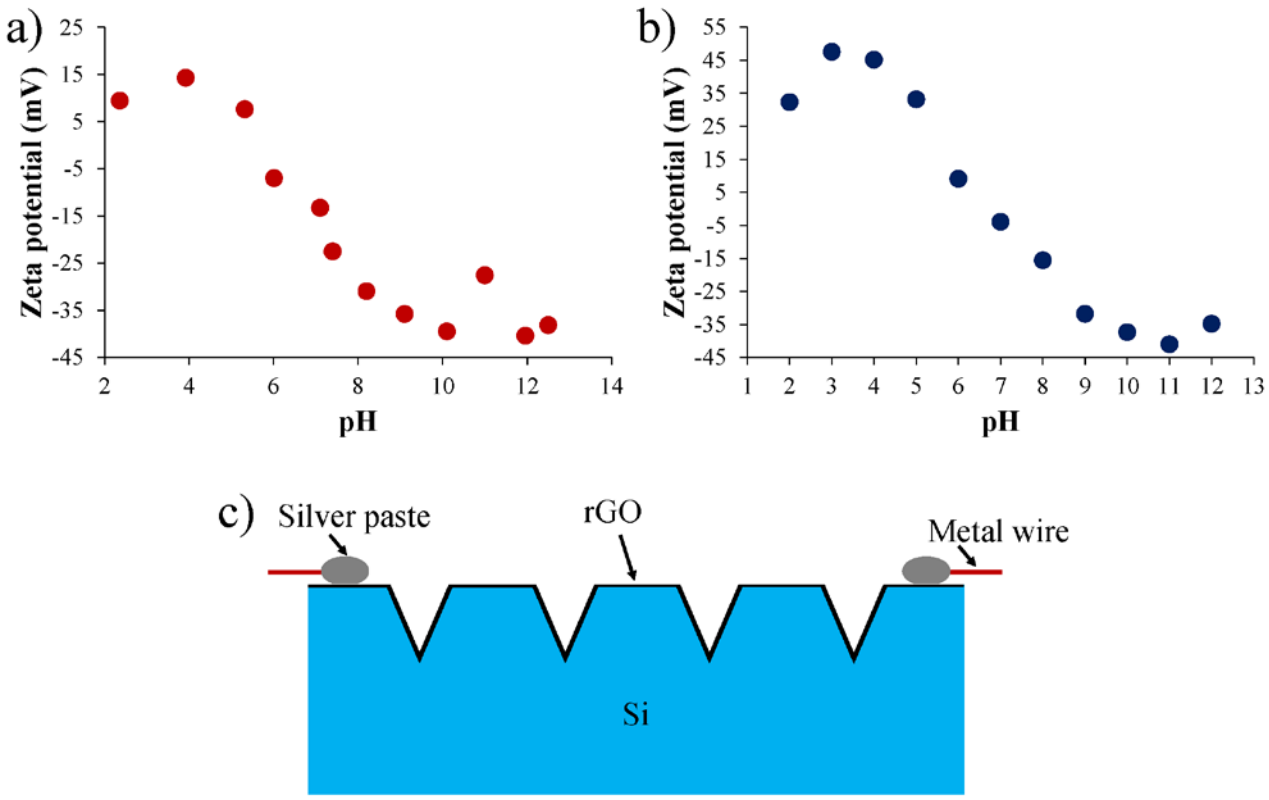

Figure 4. a) pH dependence of a lysozyme-rGO solution. The lysozyme improved the restoration of the sp^2 facilitating the reduction of the oxygen-based groups of GO (modified from ref. 96); b) pH dependence of a chitosan-rGO solution. For pH > pKa = 6.5 of chitosan, the rGO started aggregating (modified from ref. 97); c) the reverse-pyramid rGO-FET, which had a higher pH sensitivity than the rGO-FET because of the increased sensitive area. An oxygen plasma treatment further improved the sensitivity. (modified from ref. 104).

Tables

Table 1. Concentrations and ionic strengths of the solutions used to determine the effects of different electrolytes. The buffers were obtained in 0.05 M phosphate solutions, and 0.05 M potassium was present in chloride and sodium solutions (adapted from ref. 42).

Electrolyte	pH	Concentration (M)	Ionic strength (M)
Na^+	6	0.0056	0.1224
	7	0.0279	0.2116
	8	0.0463	0.2852
K^+	6	0.0556	0.1224
	7	0.0779	0.2116
	8	0.0963	0.2852
Cl^-	6	0.0444	0.2112
	7	0.0221	0.2558
	8	0.0037	0.2926

1082 Table 2. Characteristics of the graphene and rGO field effect transistors for measuring pH.

FET Configuration	Substrate	V_G (V)	V_{DS} (V)	Sensitivity (mV/pH)	pH range	Ref.
Solution-gated	6H-SiC	[-1, 1]	-1	99	[2, 12]	36
Gate-free	SiO_2/Si	Not applicable	Not reported	2.13 KΩ/pH	[4, 10]	37
Gate-free	Paper	Not applicable	[-1, 1]	30.8 Ω/pH	[1 10.5]	38
Solution-gated	SiO_2/Si	[-0.05, 0.05]	Not reported	30	[4, 8.2]	39
Solution-gated	6H–SiC	[-1.2, 0.3]	-0.05	19	[3, 12]	40
Solution-gated, suspended graphene	SiO_2/Si	[-0.05, 0.05]	Not reported	17	[6, 9]	41
Solution-gated	SiO_2/Si	[0, 1]	0.05	-78, -38 and -7 for 0.05 M Na^+, Cl^- and K^+ solutions, respectively. +69 for reference buffers	[6, 8]	42
Solution-gated	SiO_2/Si	[0.1, 0.8]	[0.01, 0.05]	6	[5, 10]	44
Solution-gated, graphene mesh	SiO_2/Si	[-0.1, 0.6]	0.05	90 (single use) 7 (after 3 cycles)	[6.55, 8.25]	45
Solution-gated, graphene nanoribbons	SiO_2/Si	[0.07, 0.32]	0.01	23.6	[6, 8]	46
Solution-gated, suspended graphene nanoribbons	SiO_2/Si	[-1.8, 1.8]	1	25	[5, 9]	47

Solution-gated, anodized graphene	SiC		Not reported	51.3	2 and 10	48
Solution-gated	SiO_2/Si, PEN	[-0.1, 0.5]	50	22 (both substrates)	[4, 8]	53
Solid gate, HfO_2 dielectric	SiO_2/Si	[0.6, 1.6]	Not reported	57.5	[5.3, 9.3]	55
Solid gate, 3D graphene	SiO_2/Si	[-1.5, 1.5]	0.5	79 ± 7	[3, 9]	56, 57
Solution-gated, APTES treatment, rGO	SiO_2/Si	[-0.2, 0.2]	0.1	29	[6, 9]	103
Solution-gated, reverse-pyramid, oxygen plasma treated, rGO	Si	[1.3, 2.4]	0.2	57	[1, 13]	104, 105

1094 Table 3. Characteristics of the graphene-base quantum dots.

Starting Material	Size (diameter, nm)	Excitation wavelength (λ_{ex}, nm)	Sensitivity	pH range	Ref.
Nitrogen-doped graphene	2.3	365	-4 (mV/pH)	[2, 9]	70
Nitrogen-doped (from L-DOPA) graphene	12.5	346	~80 (a.u. of fluorescence intensity)/pH	[3, 8]	71
Graphene (in 5 ml DMSO solution which contained 0.01 M TBAP)	10.6	365	~5 nm/pH	[1 14]	72
P7AC-b-PNIPAAm-grafted graphene	10	365	Not reported	[1, 11]	73
Graphite powder	2 and 18	250 to 390	Not reported	[2, 12]	75
PAA-CdS/ZnS and P2VP-CdSe/ZnS nanodots anchored to graphene oxide	PAA-CdS/ZnS = ~85 at pH 7 P2VP-CdSe/ZnS = ~70 nm at pH 7	365	~-0.56/pH	[1, 7]	90
Ozononized reduced graphene oxide	2–5	254	Not reported	[1, 13]	99

1095

1096